Supplementary Figures

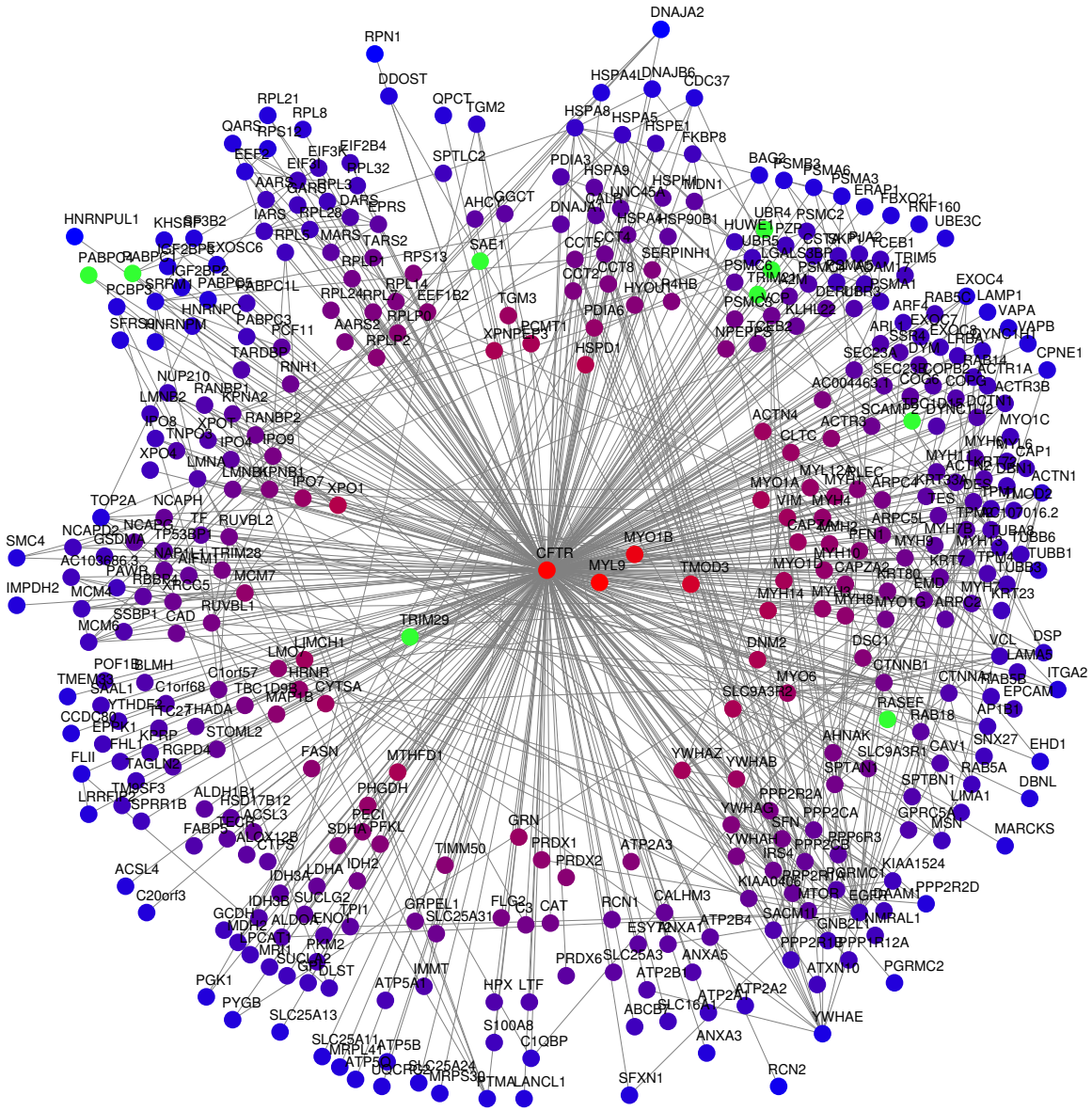

Fig. S1. Network representation of the wt CFTR core interactome. Colour and distance to the center (CFTR) reflect relative enrichment of individual interactors over background. Green colouring indicates interactors targeted for functional rescue. Proteins are grouped according to function as in Figure 1b.

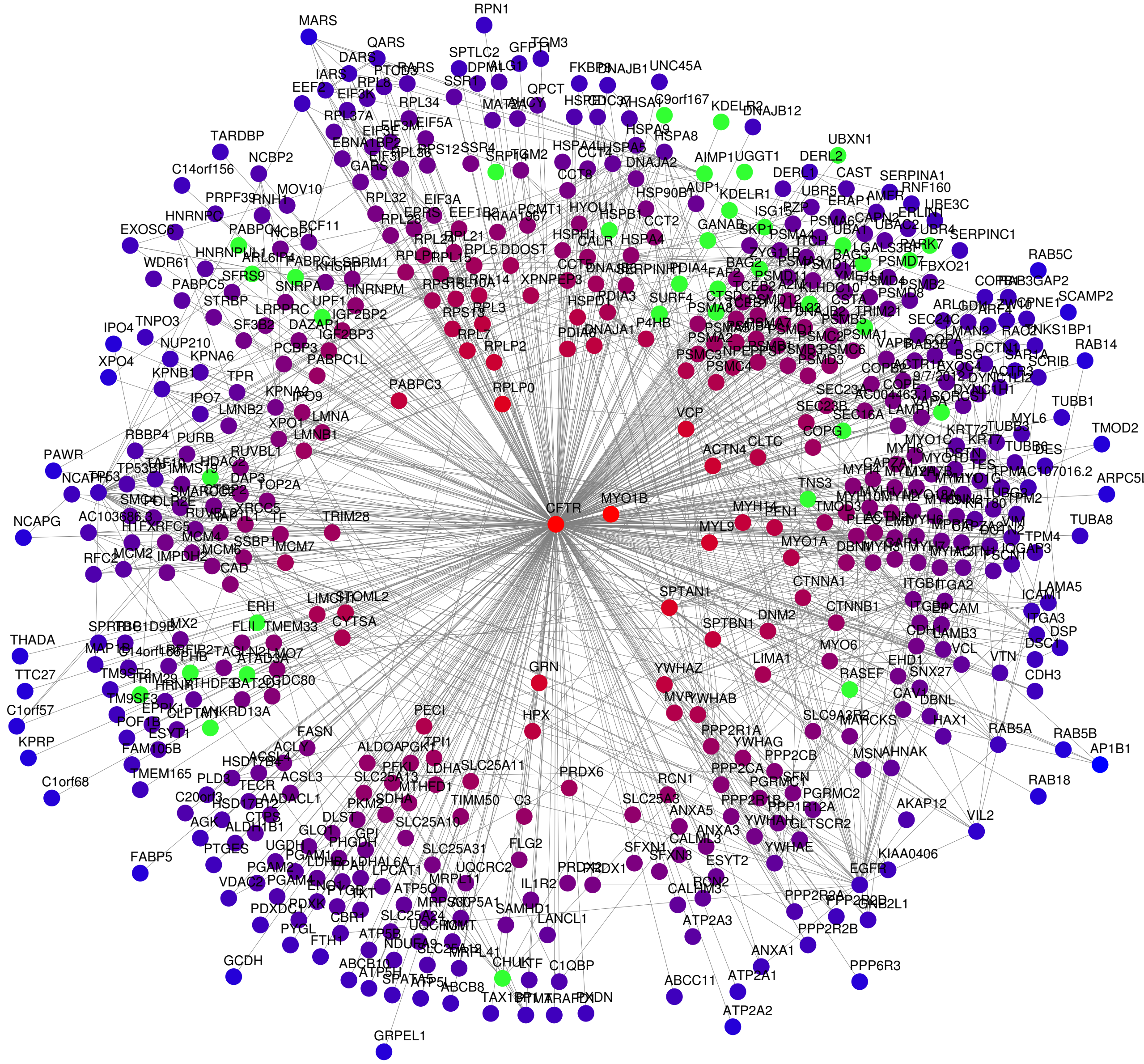

Fig. S2. Network representation of the ΔF508 CFTR core interactome. Colour and distance to the center (CFTR) reflect relative enrichment of individual interactors over background. Green colouring indicates interactors targeted for functional rescue. Proteins are grouped according to function as in Figure 1b.

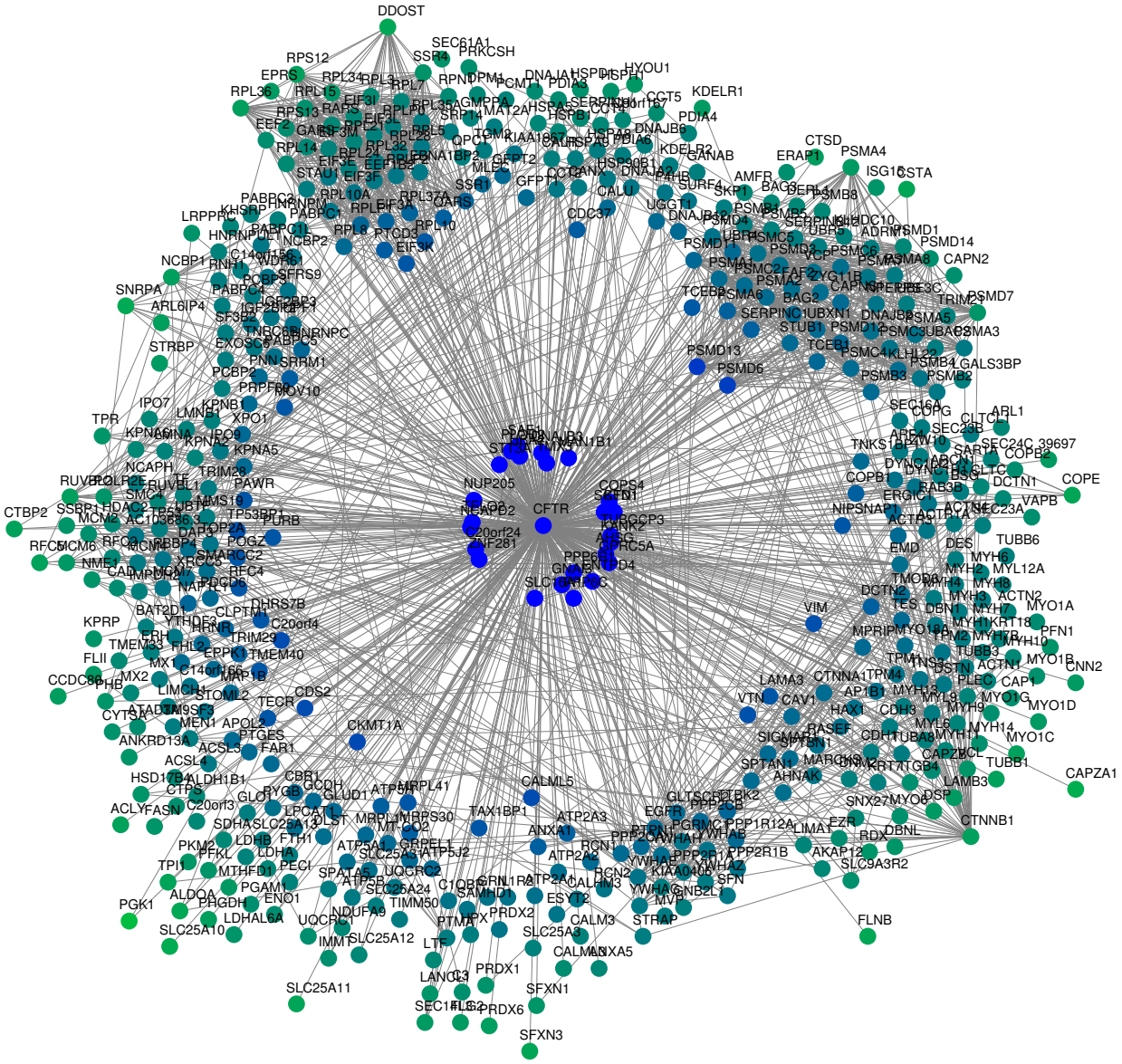

Fig. S3. Network representation of ΔF508 CFTR interactome changes occuring at 1hour after temperature shift to 30˚C. Colour and distance to CFTR indicate fold-change of individual interactors (green: reduced; blue: enhanced association). The innermost circle contains interactors gained during temperature shift. Proteins are grouped according to function as in Figure 1b.

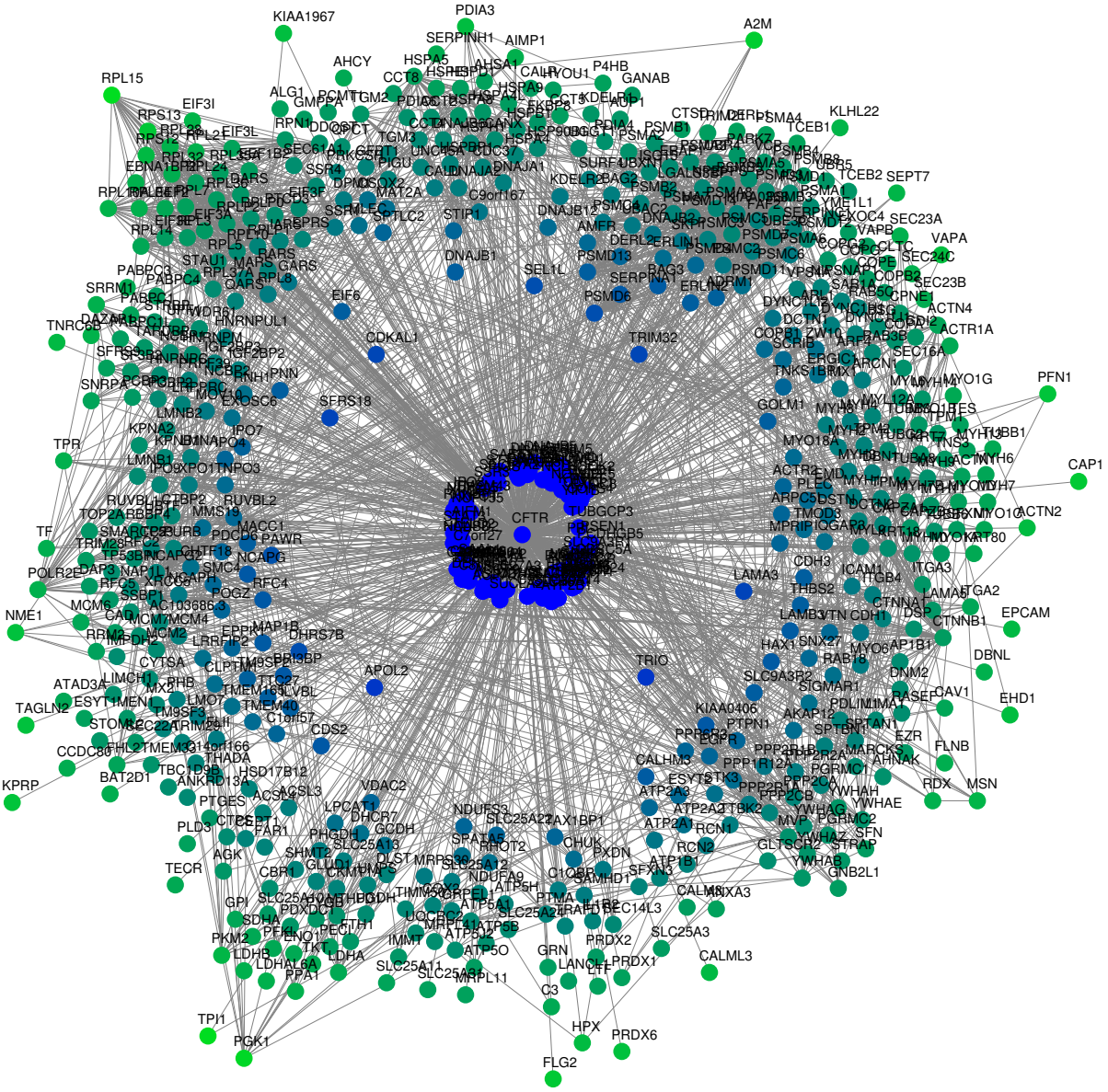

Fig. S4. Network representation of ΔF508 CFTR interactome changes occuring at 6 hours after temperature shift to 30˚C. Colour and distance to CFTR indicate fold-change of individual interactors (green: reduced; blue: enhanced association). The innermost circle contains interactors gained during temperature shift. Proteins are grouped according to function as in Figure 1b.

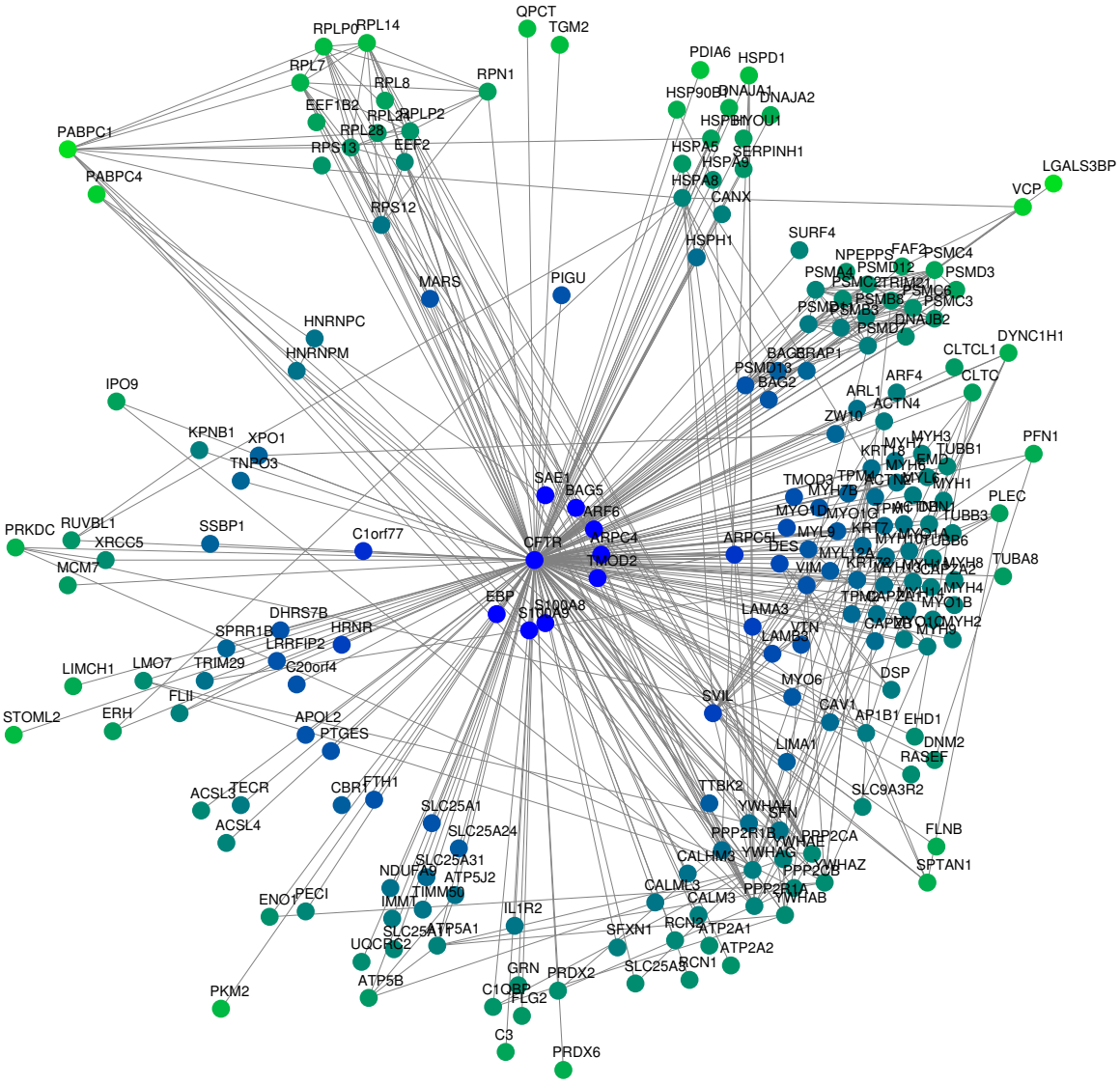

Fig. S5. Network representation of ΔF508 CFTR interactome changes occuring at 24 hours after temperature shift to 30˚C. Colour and distance to CFTR indicate fold-change of individual interactors (green: reduced; blue: enhanced association). The innermost circle contains interactors gained during temperature shift. Proteins are grouped according to function as in Figure 1b.

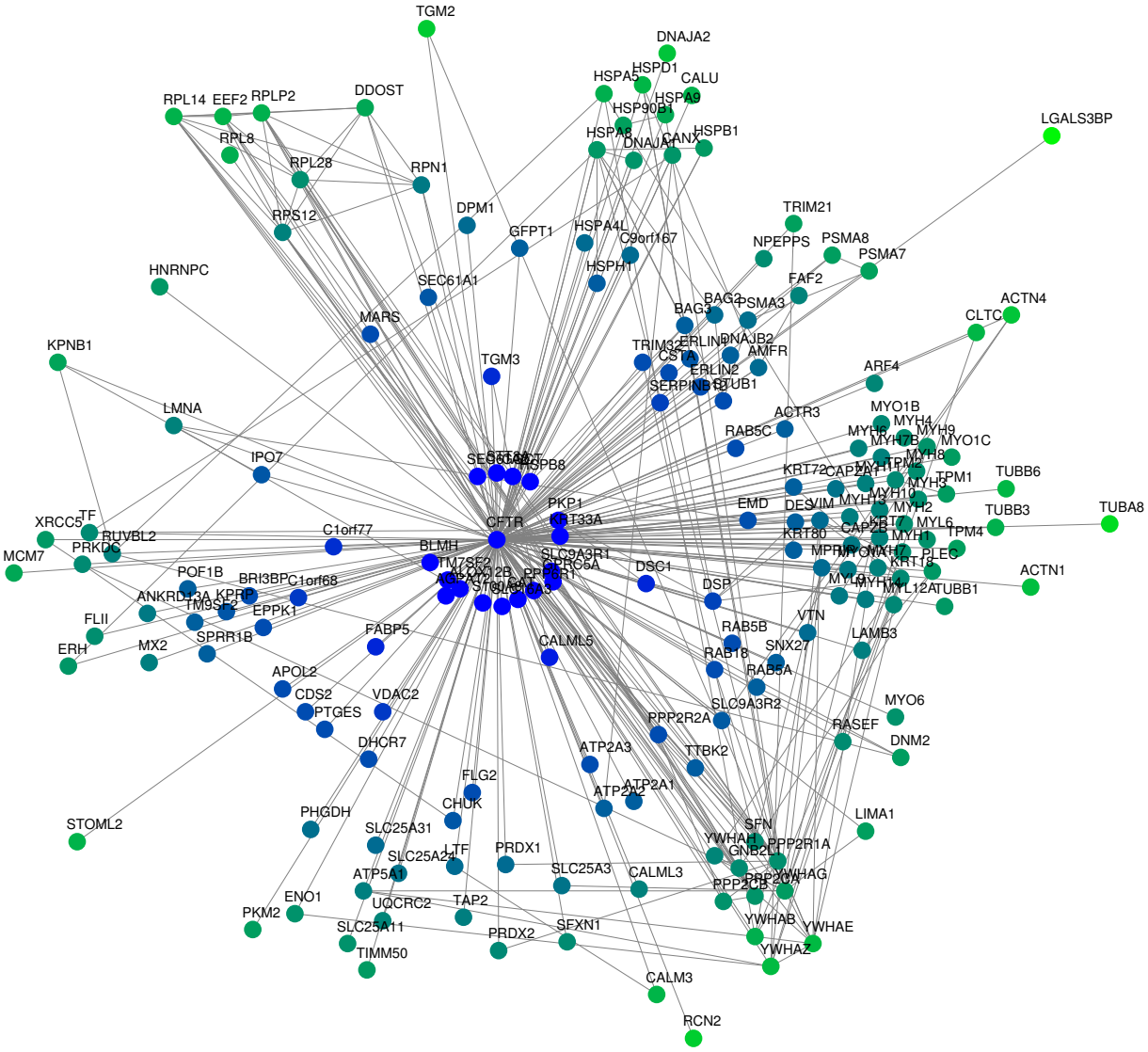

Fig. S6. Network representation of ΔF508 CFTR interactome changes occuring after returning the cells to 37˚C for 14 hours subsequent to 24 hours at 30˚C. Colour and distance to CFTR indicate fold-change of individual interactors (green: reduced; blue: enhanced association). The innermost circle contains interactors gained during temperature shift. Proteins are grouped according to function as in Figure 1b.

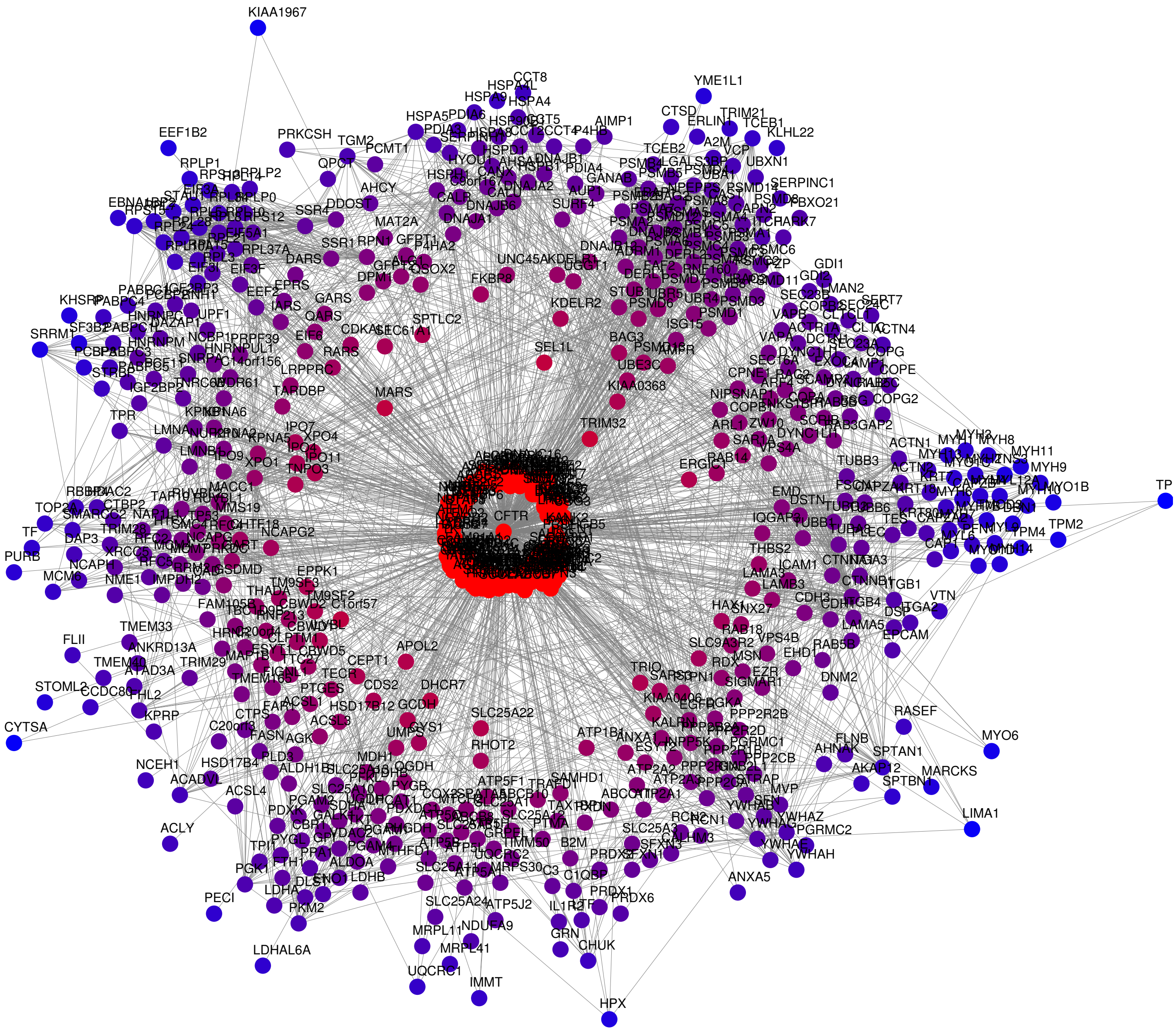

Fig. S7. Network representation of dynamic changes in the ΔF508 CFTR interactome upon treatment with 5 μM SAHA for 24 h. Distance to ΔF508 CFTR and colour represent fold-change of individual interactors (blue: reduced; red: enhanced). Proteins are grouped according to function as in Figure 3a.

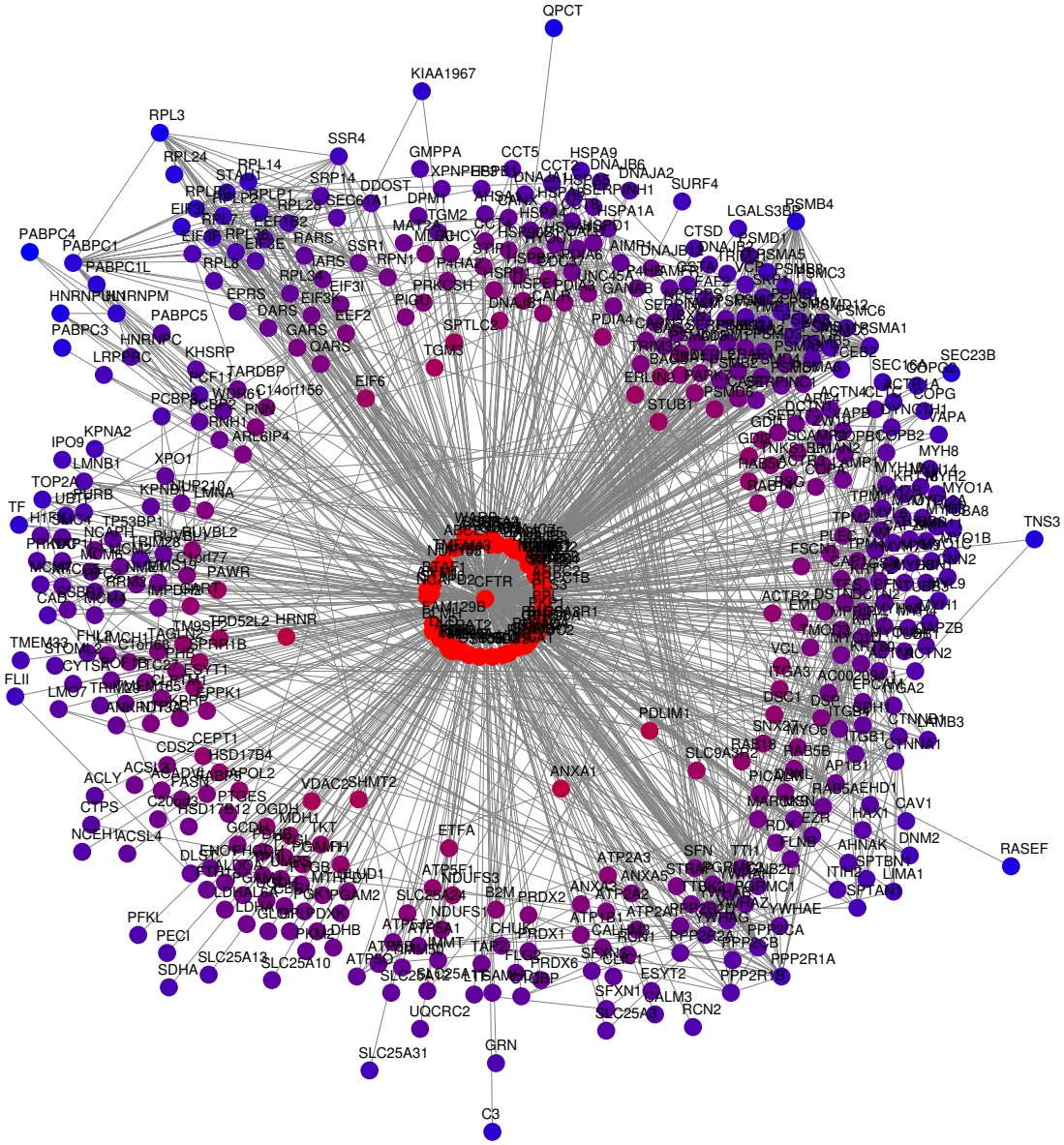

Fig. S8. Network representation of dynamic changes in the ΔF508 CFTR interactome upon treatment with 100 nM TSA for 24 h. Distance to ΔF508 CFTR and colour represent fold-change of individual interactors (blue: reduced; red: enhanced). Proteins are grouped according to function as in Figure 3a.

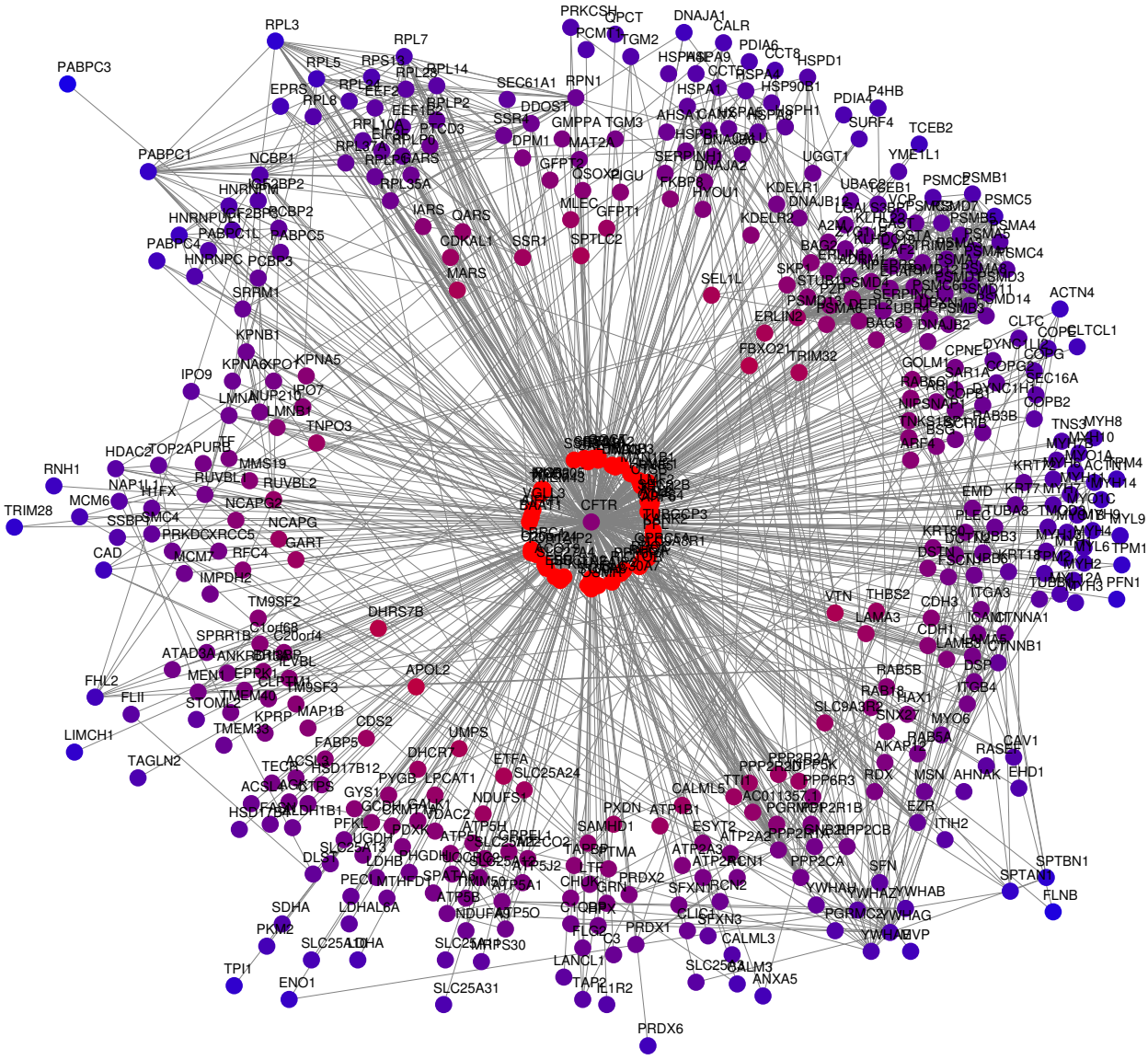

Fig. S9. Network representation of dynamic changes in the ΔF508 CFTR interactome upon siRNA mediated knockdown of HDAC7. Distance to ΔF508 CFTR and colour represent fold-change of individual interactors (blue: reduced; red: enhanced). Proteins are grouped according to function as in Figure 3a.

1. Supplementary results and discussion

Remodeling of the ΔF508 CFTR interactome upon HDACi

To identify the mechanisms by which HDAC inhibition mediates ΔF508 CFTR rescue, CFBE41o- cells were treated with 100 nM Trichostatin A (TSA) or 5 μM Suberoylanilide hydroxamic acid (SAHA) for 24 h. Both HDAC inhibitors affect class I and II HDACs [41]. In addition, HDAC7 was knocked down by siRNA mediated RNAi. All three treatments induced large-scale changes of the ΔF508 CFTR interactome, altering 35%-50% of all interactions (Supplementary Tables S11-13). The treatment with 5 μM SAHA for 24 h induced the largest change to the ΔF508 CFTR interactome (Figure 3a, top panel, Supplementary tables S14-S16) differentially down-regulating 213 proteins by more than 3-fold (excluded by the circle in blue) and abolishing interactions with 81 proteins (not depicted in the network), while up- regulating interactions with 49 proteins by at least 3-fold (included within the red circle) and recruiting an additional 144 proteins to the ΔF508 CFTR interactome, of which 31 are also present in the wt CFTR interactome (innermost circle of proteins). In contrast, HDAC7 siRNA knockdown induced the least number of changes to the ΔF508 CFTR interactome, down-regulating 125 proteins by more than 3-fold (excluded by the circle in blue) and abolishing interactions with 108 proteins, while up-regulating interactions with only 13 proteins by more than 3-fold and recruiting an additional 48 proteins, of which 12 are present in the non-mutated CFTR interactome (included within the red circle) (Figure 3a, lower panel, Supplementary table S14). Those perturbations are effectively molecular pathways that permit a more wt CFTR-like biogenesis of ΔF508 CFTR.

Sub-networks of interactors selected for RNAi

Candidates for the RNAi screen were selected according to the following criteria: (1) target interaction profiles (Extended Data Figure 4a), (2) abundance of candidate target proteins, (3) confidence of belonging to the core interactome, (4) significance of change upon temperature shift or HDACi (>=2σ cutoff), as well

as (5) relational information about protein function and subcellular localization. Upon knockdown of the candidates, appearance of fully glycosylated ΔF508 CFTR (band C) was used to assess completion of glycosylation in the Golgi as an indicator for rescue of ΔF508 CFTR maturation, whereas the amount of total ΔF508 CFTR protein relative to control was used to assess changes in ΔF508 CFTR protein production. It can be argued that an increase in band B alone is likely to also lead to an increase in band C as a consequence of increased ΔF508 CFTR protein. However, increase in band B is not necessarily accompanied by the appearance of band C as shown by the example of ARL6IP4 and SIN3B knockdown. In addition, several target proteins showed increased ratios of band C to band A/B without or only marginal concomitant increase in band B.

Many of the 31 novel interactors whose knockdown promoted ΔF508 CFTR maturation belong to distinct protein complexes or form distinct sub-networks (Fig. 4b), which can be grouped into five categories:

(1) mRNA decay and co-translational control network

The screen surprisingly identified a remarkable number of proteins involved in mRNA stabilization and translation that were overrepresented in ΔF508 CFTR IPs and whose interaction was strongly sensitive to both temperature shift and HDACi. Five of the 15 most consistently regulated and more abundant CFTR interactors in this group were poly-A binding protein, cytoplasmic 1 (PABPC1), poly-A binding protein, cytoplasmic 4 (PABPC4), polypyrimidine tract binding protein 1 (PTBP1), UPF1 regulator of nonsense transcripts homolog (yeast) (UPF1), and Y box binding protein 1 (YBX1), - none of which have been associated with CFTR biogenesis before. These five proteins form an extensive network together with other identified RNA processing proteins with similar interaction profiles as well as with proteins involved in translational control and the N-end-rule pathway. Strikingly, all of these proteins are implicated in translational silencing and can control mRNA degradation through divergent pathways of small RNA-mediated silencing, poly-A induced degradation or by

stimulating exonuclease-mediated mRNA degradation [42-44]. Recently, it was also shown that PABP (PABPC1) is required for de-adenylation [43]. Since the knockdowns of PABPC1, PABPC4, PTBP1, UPF1 and YBX1 all strongly increased appearance of band C and some also increased band B we suggest that this network controls ΔF508 CFTR translation by regulating its mRNA stability, perhaps depending on the progress of insertion into the ER membrane. Indeed, we identified three AU-rich elements in the 3'UTR and four AUUUA pentamers within its coding sequence (NM_000492, nt 372-376, nt 494-498, nt, 2884-2886, nt 4071-4075, nt 4806-4810, nt 5533-5537, nt 5698-5710, and (Baudouin-Legros et al., 2005) which are preserved in CFBE41o- cells. These elements are prime regulators of RNA stability and can repress translation [45,46]. In addition, a translational inhibitor of labile mRNAs, TIA-1 [47], which recognizes AU-rich elements and other mRNA destabilizing elements (polypyrimidine tracts) was detected only in the ΔF508 CFTR IPs.

(2) Novel Hsp90 chaperone complex and ER quality control components

The next step in CFTR biogenesis that was affected by shRNA knockdown of interactors, is the protein folding process and ER quality control. We uncovered that disturbing the interaction of ΔF508 CFTR with the protein tyrosine phosphatase-like A domain containing 1 (PTPLAD1) protein is critical for correct CFTR maturation, - most likely by influencing CFTR folding since PTPLAD1, also known as B-IND1, exhibits Hsp90 co-chaperone activity, is capable of binding to FKBP8 and is involved in recycling of the Hsp90 chaperone complex [48]. Its knockdown strongly enhanced ΔF508 CFTR maturation, suggesting that it may limit the availability of the HSP90 chaperone complex for folding of ΔF508 CFTR or alternatively the accessibility of the folding machinery to ΔF508 CFTR. Another ΔF508 CFTR interactor, which is potentially involved in modulating the ΔF508 CFTR folding process, is the protein disulfide isomerase family A member 4 (PDIA4). PDIA4 is part of an ER complex containing BiP, GRP94, UDP-GT, GRP170 and PDI that recognizes unfolded protein regions and subsequently retains such proteins in the ER, presumably for re-folding [49]. The

enhanced maturation of ΔF508 CFTR upon knockdown of PDIA4 suggests that PDIA4 is probably involved in partial unfolding of the protein by reducing the disulfide bonds normally formed in the CFTR protein [50,51] and is part of the ER-quality control that channels misfolded proteins to ERAD. In line with disturbed folding and enhanced ER quality control, we also detected enhanced association of the ER-resident enzymes UGGT1, PRKCSH, and GANAB, which are involved in N-glycosylation and influence interaction of glycoproteins with the lectin-chaperones calnexin and calreticulin. We therefore tested knockdown of PRKCSH, GANAB and UGGT1. While knockdown of UGGT1 and GANAB did not significantly improve ΔF508 CFTR maturation, knockdown of PRKCSH, which encodes the b subunit of glucosidase II, positively influenced ΔF508 CFTR maturation. However, its effect was rather weak when compared to rescue mediated by knockdown of other interactors, indicating that it is not enough to disturb ER quality control for correction of the CF defect.

(3) Sub-complexes influencing ΔF508 CFTR trafficking

The RNAi screen further identified several potential small sub-complexes that affect ΔF508 CFTR trafficking. One potential sub-complex is the Surf4-KDEL complex. The Surfeit 4 (SURF4) protein specifically and abundantly interacted with ΔF508 CFTR and its knockdown induced band C, the fully glycosylated and mature form of CFTR, without concomitant increase in band B. In *S. cerevisiae* the Surf4 homologue ERvp29 functions as a cargo receptor involved in protein sorting, and its knockout induces stabilization of misfolded soluble proteins [52,53]. In mammalian cells, Surf4 co-localizes with KDEL receptors and is part of the early secretory pathway and its knockdown affects retrograde transport from the cis-Golgi to ERGIC [54]. Since also the knockdown of KDELR1, KDELR2 and KDELR3 in CFBE41o- cells each stabilized ΔF508 CFTR and led to enhanced maturation of ΔF508 CFTR, Surf4 and KDEL-receptors might form a small network that retains ΔF508 CFTR and is involved in ΔF508 CFTR retrograde transport together with COP proteins. Additionally, knockdown of glutaminyl-peptide cyclotransferase (QPCT) influenced formation of band C. QPCT

Isoenzymes have been identified in the Golgi and late secretory pathway and the observed effect on ΔF508 CFTR maturation may be due to altered retention of CFTR [55], or altered aggregation as inhibition of QPCT has been shown to reduce plaque formation and improve memory and learning in mouse models of Alzheimer's disease [56] by preventing the formation of pyroglutamate residues, which block the N-terminus and enhance the aggregation propensity of beta-amyloid peptides [57]. In addition, the RNAi screen identified two more interactors that potentially influence CFTR maturation by altering its trafficking, namely the PDZ domain containing protein GIPC1, and the RAS and EF-hand domain containing GTPase (RASEF). Knockdown of both GIPC1 and RASEF was found to enhance the ratio of band C to band A/B. GIPC1 has been described as endocytic adapter, which regulates trafficking of cell surface receptors and their lysosomal degradation [58]. The function of RASEF has been little characterized, but it belongs to the Rab GTPAse family, which contains important regulators of membrane trafficking and thus may influence ΔF508 CFTR trafficking.

(4) ΔF508 CFTR degradation network

The Co-IP experiments also allowed us to define a novel, potential ΔF508 CFTR-specific degradation network (Fig. 4b). The ΔF508 CFTR specific interactome is highly enriched for proteins involved in ubiquitin mediated degradation and approximately 25% of the ΔF508 CFTR-specific interactions occur with proteins directly associated with the ubiquitin pathway or the ERAD pathway mirroring mis-processing and enhanced degradation of ΔF508 CFTR. It is well established that ΔF508 CFTR is readily degraded, but only part of the proteins are known that are involved in this process. The acquired data reveal this network for the first time and suggest that alternative pathways, in addition to the known components of the classical ERAD pathway, are involved both in wt and ΔF508 CFTR degradation and are potentially functionally redundant. A novel CFTR interactor, whose knockdown caused rescue of ΔF508 CFTR, was the potential E3-ligase TRIM21 [59]. TRIM21 is one of the most abundant interactors and binds equally to non-mutated and ΔF508 CFTR. Furthermore, knockdown of

U-box domain 8 (FAF2, also called UBXD8), kelch domain containing 10 (KLHDC10) and ubiquitin protein ligase E3 component n-recognin 4 (UBR4) all protected CFTR from degradation, and permitted partial maturation as visualized by appearance of band C. KLHDC10 and FAF2 have recently been described as Cullin2 interactors [60,61], and may be associated with the E3-ubiquitin-ligase-complex Zyg11B-Cul2-TCEB1 [62,63]. In addition, FAF2 has been shown to bind lectin, galactoside-binding, soluble, 3 binding protein (LGALS3BP) [61], which - if knocked down - decreased CFTR stability dramatically to the point where ΔF508 CFTR was no longer detectable by Western blot in CFBE41o- cells, suggesting that it counter-balances CFTR degradation by yet unknown mechanisms. In contrast, UBR4 is an E3-ligase that is part of the N-end rule pathway that recognizes destabilizing N-terminal residues according to the N-end rule and subsequently interacts with the ubiquitin system [64] and Cul2 to deliver target proteins to the proteasomal degradation machinery. In addition, UBR4, also named p600, localizes to the ER in CNS neurons [65] and has been identified as a calmodulin binding protein important for membrane morphogenesis [66]. Thus, UBR4 might be important for coupling ΔF508 CFTR to the degradation machinery in the ER and the data suggest that degradation of ΔF508 CFTR might take place as early as its N-glycosylation occurs. Although none of these proteins have been described as interacting with non-mutated CFTR or ΔF508 CFTR, FAF2 has been implicated in the dislocation of misfolded glycoproteins [63]. Other E3-ligases and ubiquitin-associated proteins were also only detected in ΔF508 CFTR-IPs like Itch and Trim32 or UBXN1, UBAC2 and the E1-ligase UBA1, which catalyzes the first step of the ubiquitin conjugation process and recruits the E2 [67-69].

Supplementary References

41 Glick, R. D. *et al.* Hybrid polar histone deacetylase inhibitor induces apoptosis and CD95/CD95 ligand expression in human neuroblastoma. *Cancer Res* **59**, 4392-4399, (1999).

42 LaCava, J. *et al.* RNA degradation by the exosome is promoted by a nuclear polyadenylation complex. *Cell* **121**, 713-724, (2005).

43 Fabian, M. R. *et al.* Mammalian miRNA RISC recruits CAF1 and PABP to affect PABP-dependent deadenylation. *Mol Cell* **35**, 868-880, (2009).
44 Garneau, N. L., Wilusz, J. & Wilusz, C. J. The highways and byways of mRNA decay. *Nat Rev Mol Cell Biol* **8**, 113-126, (2007).
45 Barreau, C., Paillard, L. & Osborne, H. B. AU-rich elements and associated factors: are there unifying principles? *Nucleic Acids Res* **33**, 7138-7150, (2005).
46 Caput, D. *et al.* Identification of a common nucleotide sequence in the 3'-untranslated region of mRNA molecules specifying inflammatory mediators. *Proc Natl Acad Sci U S A* **83**, 1670-1674, (1986).
47 Yamasaki, S., Stoecklin, G., Kedersha, N., Simarro, M. & Anderson, P. T-cell intracellular antigen-1 (TIA-1)-induced translational silencing promotes the decay of selected mRNAs. *J Biol Chem* **282**, 30070-30077, (2007).
48 Taguwa, S. *et al.* Cochaperone activity of human butyrate-induced transcript 1 facilitates hepatitis C virus replication through an Hsp90-dependent pathway. *J Virol* **83**, 10427-10436, (2009).
49 Forster, M. L. *et al.* Protein disulfide isomerase-like proteins play opposing roles during retrotranslocation. *J Cell Biol* **173**, 853-859, (2006).
50 Partridge, A. W., Melnyk, R. A. & Deber, C. M. Polar residues in membrane domains of proteins: molecular basis for helix-helix association in a mutant CFTR transmembrane segment. *Biochemistry* **41**, 3647-3653, (2002).
51 Therien, A. G., Grant, F. E. & Deber, C. M. Interhelical hydrogen bonds in the CFTR membrane domain. *Nat Struct Biol* **8**, 597-601, (2001).
52 Caldwell, S. R., Hill, K. J. & Cooper, A. A. Degradation of endoplasmic reticulum (ER) quality control substrates requires transport between the ER and Golgi. *J Biol Chem* **276**, 23296-23303, (2001).
53 Belden, W. J. & Barlowe, C. Role of Erv29p in collecting soluble secretory proteins into ER-derived transport vesicles. *Science* **294**, 1528-1531, (2001).
54 Mitrovic, S., Ben-Tekaya, H., Koegler, E., Gruenberg, J. & Hauri, H. P. The cargo receptors Surf4, endoplasmic reticulum-Golgi intermediate compartment (ERGIC)-53, and p25 are required to maintain the architecture of ERGIC and Golgi. *Mol Biol Cell* **19**, 1976-1990, (2008).
55 Cynis, H. *et al.* Isolation of an isoenzyme of human glutaminyl cyclase: retention in the Golgi complex suggests involvement in the protein maturation machinery. *J Mol Biol* **379**, 966-980, (2008).
56 Schilling, S. *et al.* Glutaminyl cyclase inhibition attenuates pyroglutamate Abeta and Alzheimer's disease-like pathology. *Nat Med* **14**, 1106-1111, (2008).
57 Saido, T. C. *et al.* Dominant and differential deposition of distinct beta-amyloid peptide species, A beta N3(pE), in senile plaques. *Neuron* **14**, 457-466, (1995).
58 Lee, N. Y., Ray, B., How, T. & Blobe, G. C. Endoglin promotes transforming growth factor beta-mediated Smad 1/5/8 signaling and

inhibits endothelial cell migration through its association with GIPC. *J Biol Chem* **283**, 32527-32533, (2008).
59 Mallery, D. L. *et al.* Antibodies mediate intracellular immunity through tripartite motif-containing 21 (TRIM21). *Proc Natl Acad Sci U S A* **107**, 19985-19990, (2010).
60 Behrends, C., Sowa, M. E., Gygi, S. P. & Harper, J. W. Network organization of the human autophagy system. *Nature* **466**, 68-76, (2010).
61 Alexandru, G. *et al.* UBXD7 binds multiple ubiquitin ligases and implicates p97 in HIF1alpha turnover. *Cell* **134**, 804-816, (2008).
62 Vasudevan, S., Starostina, N. G. & Kipreos, E. T. The Caenorhabditis elegans cell-cycle regulator ZYG-11 defines a conserved family of CUL-2 complex components. *EMBO Rep* **8**, 279-286, (2007).
63 Mueller, B., Klemm, E. J., Spooner, E., Claessen, J. H. & Ploegh, H. L. SEL1L nucleates a protein complex required for dislocation of misfolded glycoproteins. *Proc Natl Acad Sci U S A* **105**, 12325-12330, (2008).
64 Tasaki, T. *et al.* A family of mammalian E3 ubiquitin ligases that contain the UBR box motif and recognize N-degrons. *Mol Cell Biol* **25**, 7120-7136, (2005).
65 Shim, S. Y. *et al.* Protein 600 is a microtubule/endoplasmic reticulum-associated protein in CNS neurons. *J Neurosci* **28**, 3604-3614, (2008).
66 Nakatani, Y. *et al.* p600, a unique protein required for membrane morphogenesis and cell survival. *Proc Natl Acad Sci U S A* **102**, 15093-15098, (2005).
67 McGrath, J. P., Jentsch, S. & Varshavsky, A. UBA 1: an essential yeast gene encoding ubiquitin-activating enzyme. *Embo J* **10**, 227-236, (1991).
68 Lee, I. & Schindelin, H. Structural insights into E1-catalyzed ubiquitin activation and transfer to conjugating enzymes. *Cell* **134**, 268-278, (2008).
69 Jin, J., Li, X., Gygi, S. P. & Harper, J. W. Dual E1 activation systems for ubiquitin differentially regulate E2 enzyme charging. *Nature* **447**, 1135-1138, (2007).
70 Tiscornia, G., Singer, O. & Verma, I. M. Production and purification of lentiviral vectors. *Nat Protoc* **1**, 241-245, (2006).
71 Laemmli, U. K. Cleavage of structural proteins during the assembly of the head of bacteriophage T4. *Nature* **227**, 680-685, (1970).
72 Galietta, L. V., Jayaraman, S. & Verkman, A. S. Cell-based assay for high-throughput quantitative screening of CFTR chloride transport agonists. *Am J Physiol Cell Physiol* **281**, C1734-1742, (2001).
73 Washburn, M. P., Wolters, D. & Yates, J. R., 3rd. Large-scale analysis of the yeast proteome by multidimensional protein identification technology. *Nat Biotechnol* **19**, 242-247, (2001).
74 Xu, T. *et al.* ProLuCID, a fast and sensitive tandem mass spectra-based protein identification program. *Mol Cell Proteomics* **5**, S174, (2006).
75 Elias, J. E., Haas, W., Faherty, B. K. & Gygi, S. P. Comparative evaluation of mass spectrometry platforms used in large-scale proteomics investigations. *Nat Methods* **2**, 667-675, (2005).

76 Cociorva, D., D, L. T. & Yates, J. R. Validation of tandem mass spectrometry database search results using DTASelect. *Curr Protoc Bioinformatics* Chapter 13, Unit 13 14, (2007).
77 Li, X. J., Zhang, H., Ranish, J. A. & Aebersold, R. Automated statistical analysis of protein abundance ratios from data generated by stable-isotope dilution and tandem mass spectrometry. *Analytical chemistry* **75**, 6648-6657, (2003).
78 Ranish, J. A. *et al.* Identification of TFB5, a new component of general transcription and DNA repair factor IIH. *Nature genetics* **36**, 707-713, (2004).
79 Montojo, J. *et al.* GeneMANIA Cytoscape plugin: fast gene function predictions on the desktop. *Bioinformatics* **26**, 2927-2928, (2010).
80 Pavlopoulos, G. A., Hooper, S. D., Sifrim, A., Schneider, R. & Aerts, J. Medusa: A tool for exploring and clustering biological networks. *BMC research notes* **4**, 384, (2011).
81 Breitkreutz, B. J., Stark, C. & Tyers, M. Osprey: a network visualization system. *Genome Biol* **4**, R22, (2003).
82 Park, S. K., Venable, J. D., Xu, T. & Yates, J. R., 3rd. A quantitative analysis software tool for mass spectrometry-based proteomics. *Nat Methods* **5**, 319-322, (2008).
83 Suzuki, R. & Shimodaira, H. Pvclust: an R package for assessing the uncertainty in hierarchical clustering. *Bioinformatics* **22**, 1540-1542, (2006).
84 Wang, X. *et al.* Hsp90 cochaperone Aha1 downregulation rescues misfolding of CFTR in cystic fibrosis. *Cell* **127**, 803-815, (2006).

3. Supplementary Tables

Supplementary Table S1-S3. CFTR core interactome. All identified proteins and the simplified functional categorization used for depicting the functional groups in the networks are given (Table S1). Mapped interactions and interaction value (distance to CFTR) for wt and ΔF508 CFTR are listed in Table S2 and S3, respectively.

Supplementary Table S4. Comparison of the interactome from Wang et al, 2006 [84] with this study. Columns D and E indicate whether or not a protein identified by Wang et al, 2006 was identified as high or medium confidence interactor in this study. The table was adapted from Wang et al., 2006.

Supplementary Table S5. ΔF508 CFTR-mutation specific interactome. 208 proteins that were detected in ΔF508 CFTR IPs, but not in wt CFTR-IPs, form a mutation-specific interactome.

Supplementary Table S6. ΔF508 CFTR-mutation specific degradation network. Proteins annotated as participating in protein degradation, proteolysis, ER quality control and retrograde transport leading to degradation are listed.

Supplementary Table S7-S10. Temporal remodeling of the ΔF508 CFTR interactome during temperature shift to 30˚C. Listed are identified proteins that are high-confidence interactors and the functional classification used to generate networks. 1 h dataset (Table S7), 6 h dataset (Table S8), 24 h dataset (Table 9), 24 h reversal dataset (Table S10).

Supplementary Table S11-S13. Alterations of the ΔF508 CFTR interactome upon treatment with SAHA for 24 h (Table S11), upon treatment with TSA for 24 h (Table S12) and upon siRNA-mediated knockdown of HDAC7 in CFBE41o- cells (Table S13). Listed are identified proteins that are high-confidence interactors as well as the functional classification used to generate networks.

Supplementary Table S14. Enrichment of different cellular components in either the wt or the ΔF508 CFTR interactome using GO-analysis (GoMiner). Parent GO-terms associated with the cellular compartment are indicated.

Supplementary Table S15. shRNA sequences used for knockdown of identified interactors are identified by their TRC ID number.

Full gel scans

Figure 2b

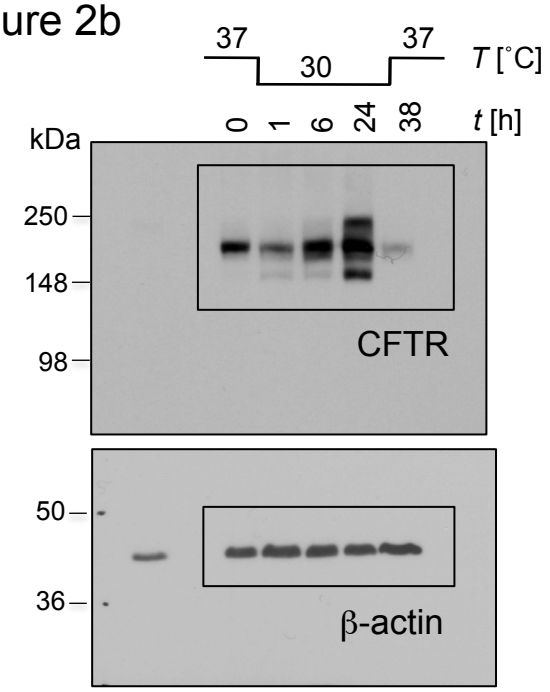

Extended Data Fig. 1

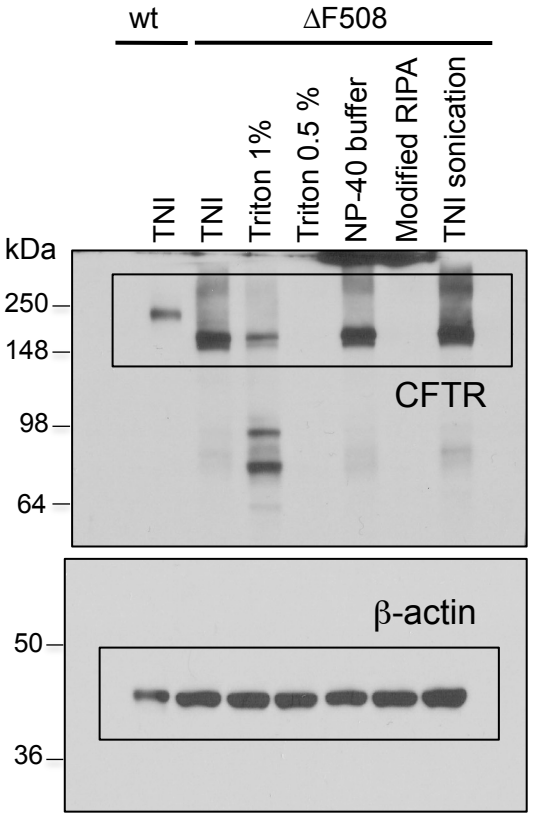

Extended Data Fig. 1

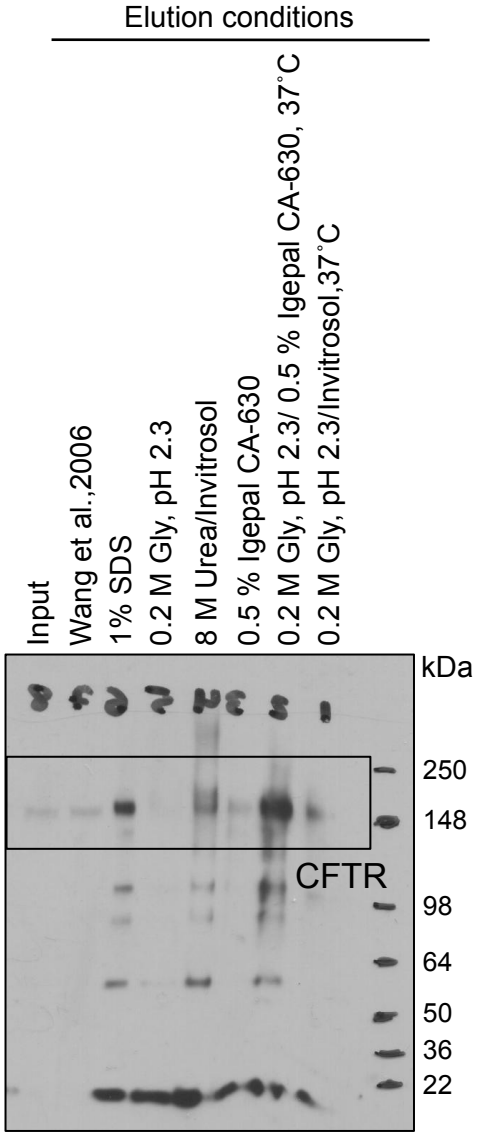

Extended Data Fig. 2c

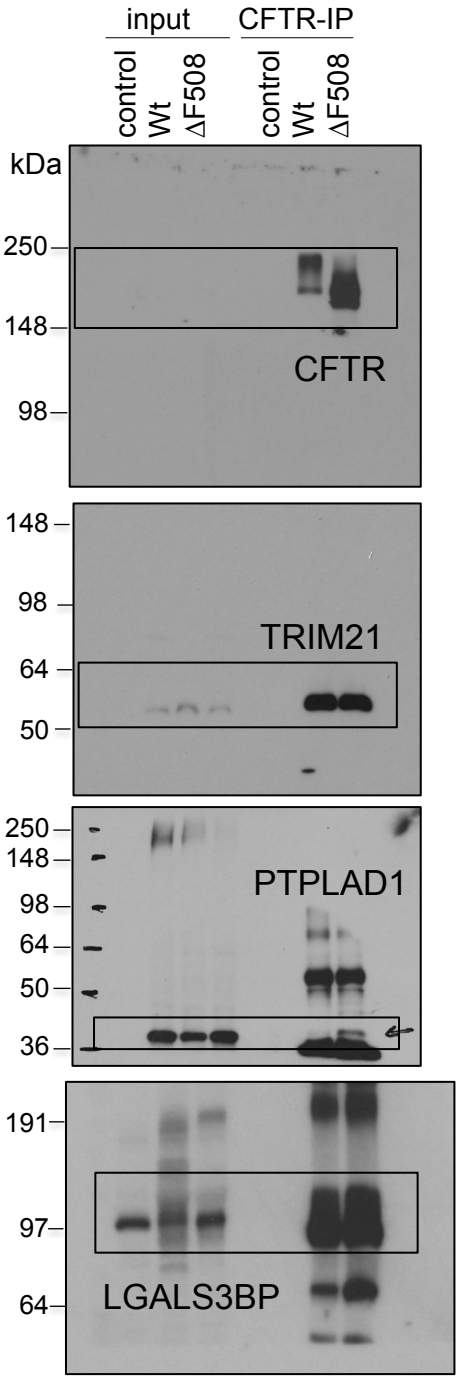

Extended Data Fig. 2d

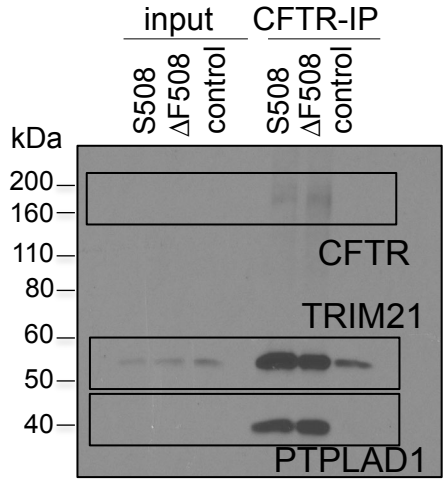

Extended Data Fig. 2d

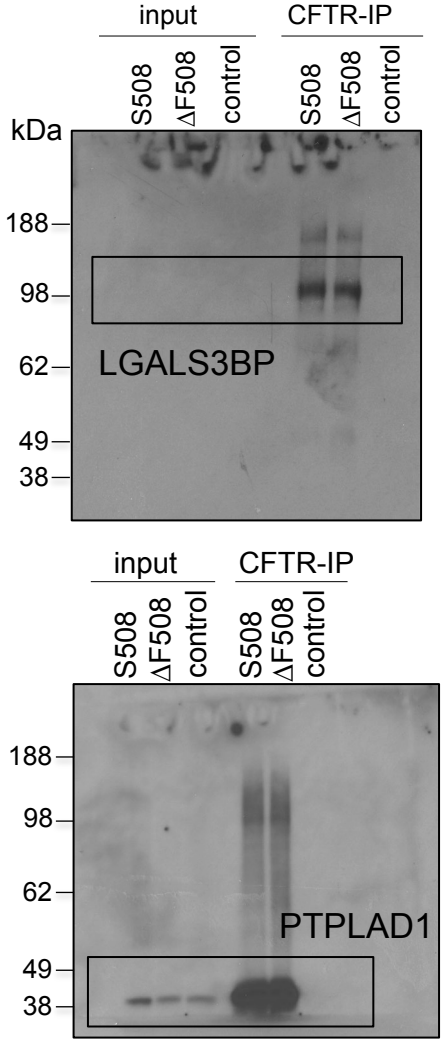

Extended Data Fig. 2g

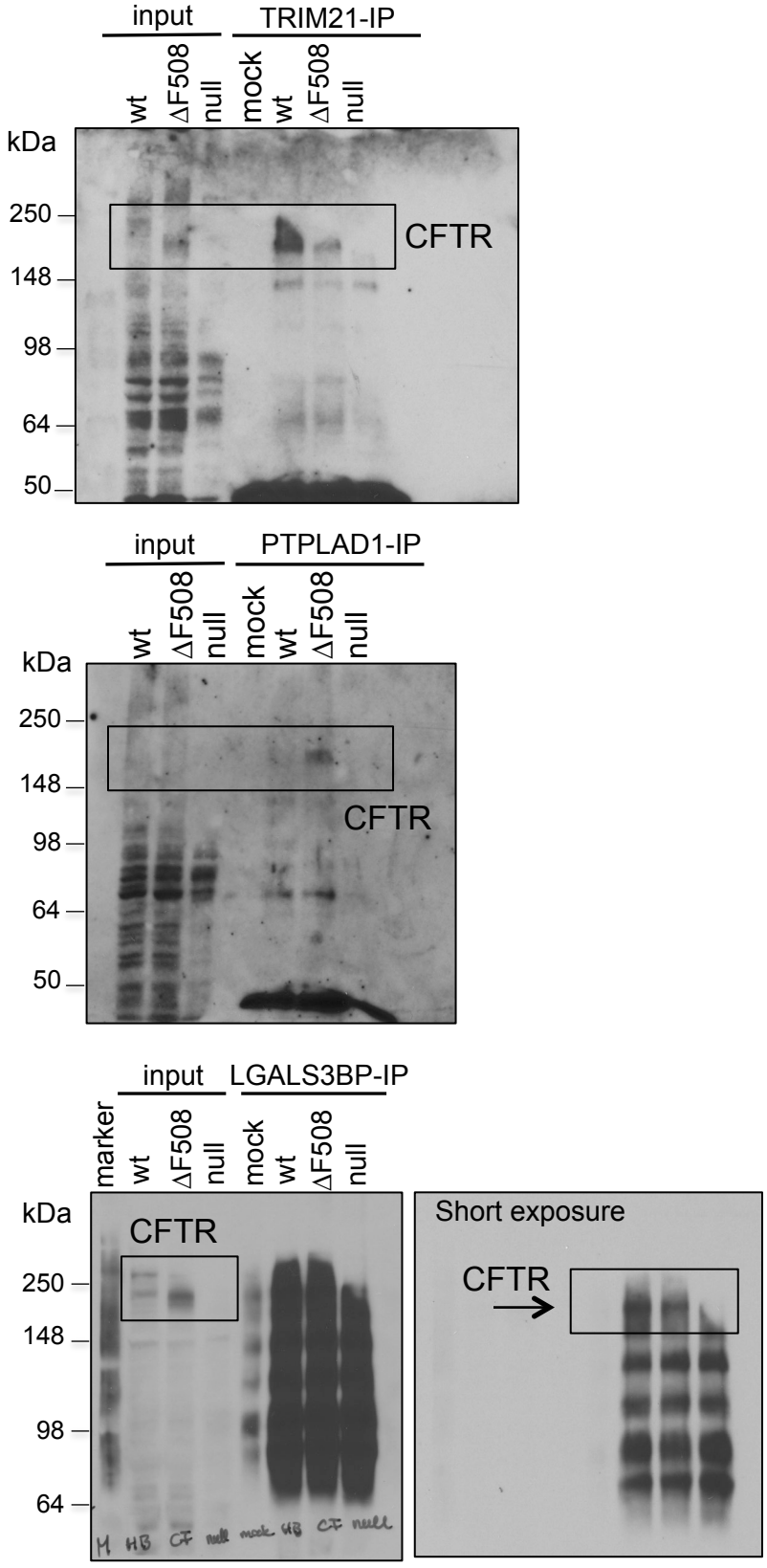

Extended Data Fig. 3

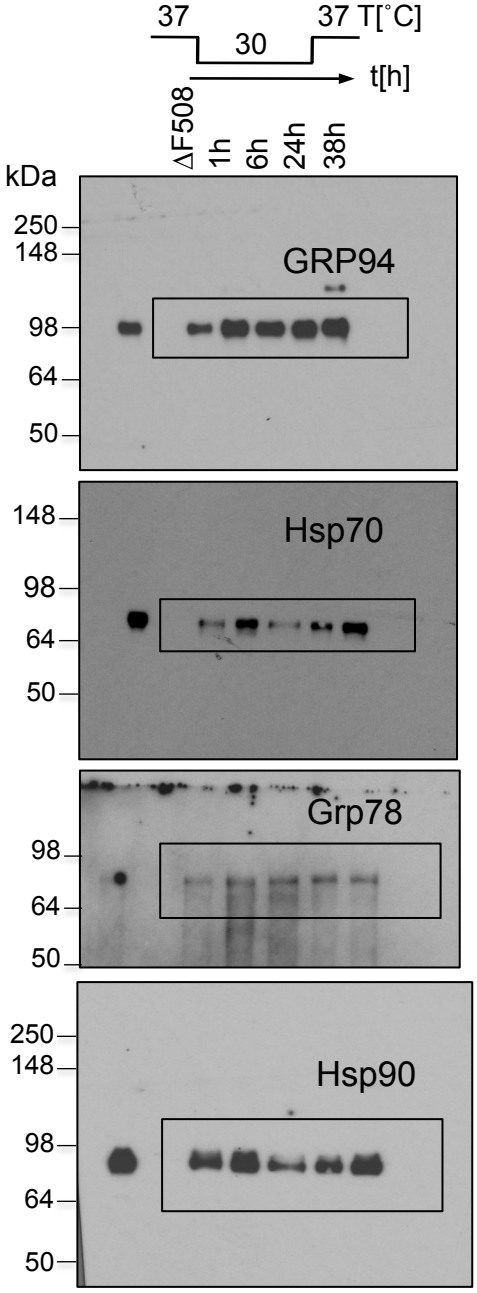

Extended Data Fig. 5

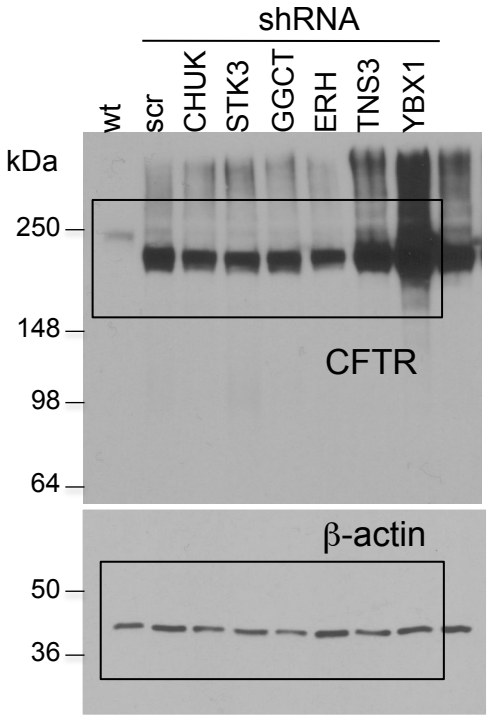

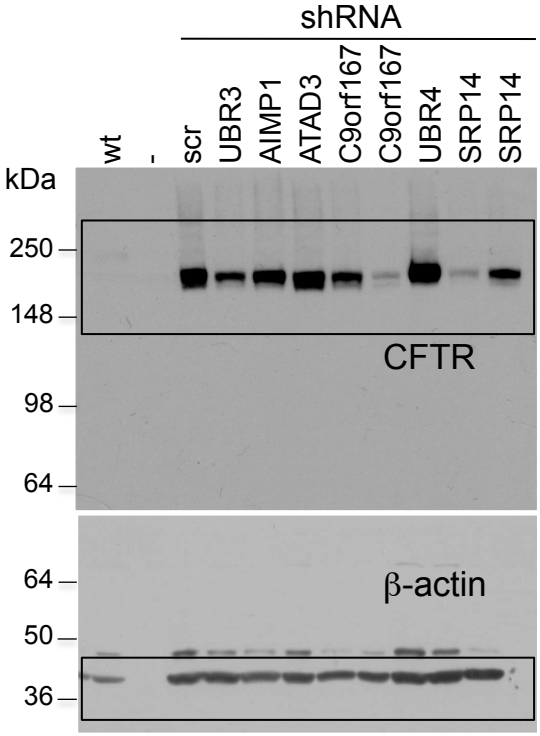

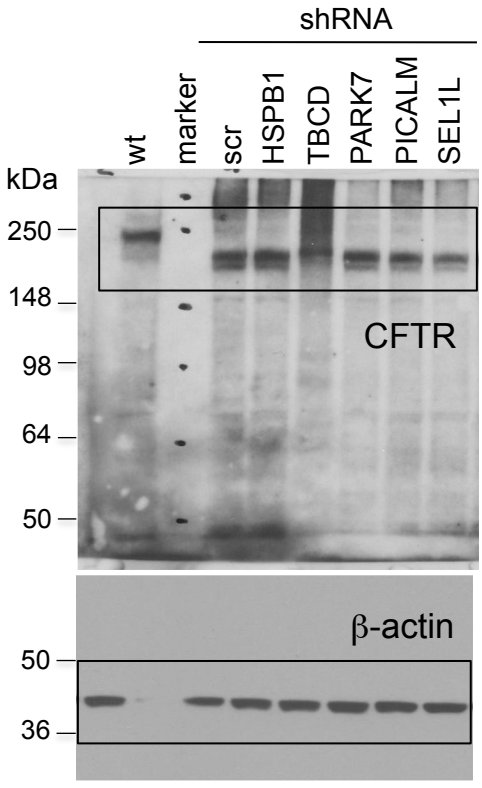

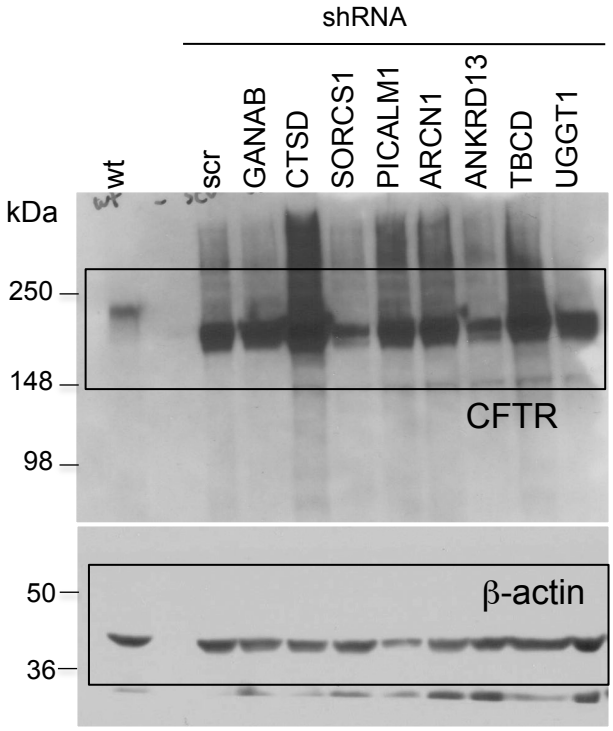

Extended Data Fig. 5

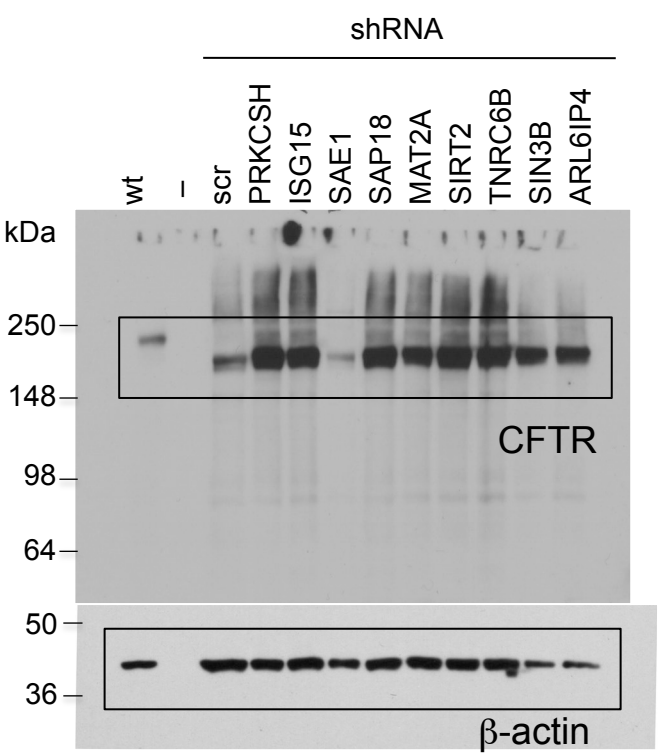

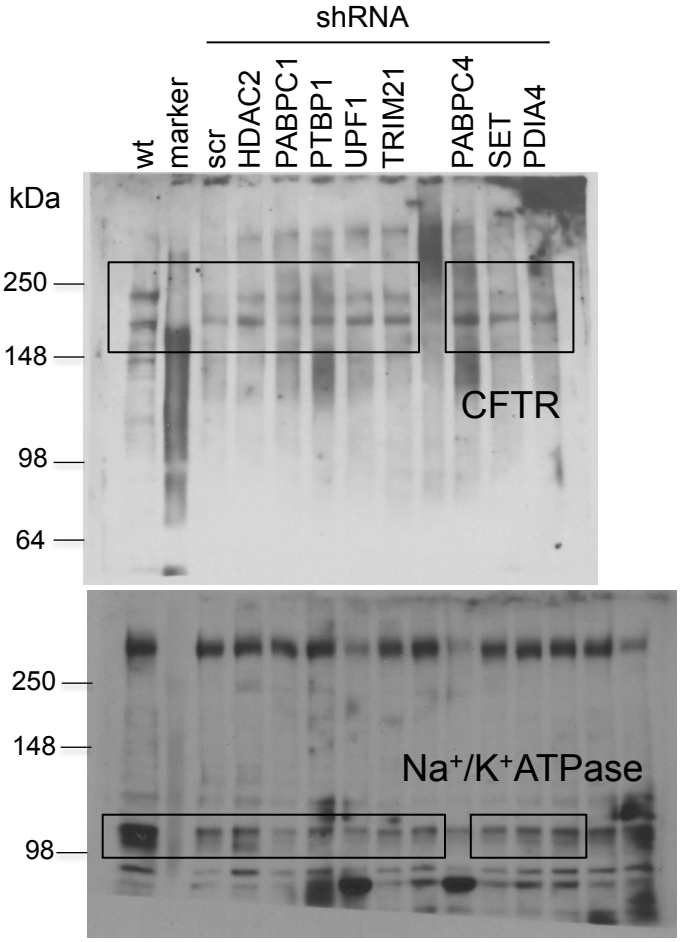

Same samples reloaded as above on a different blot

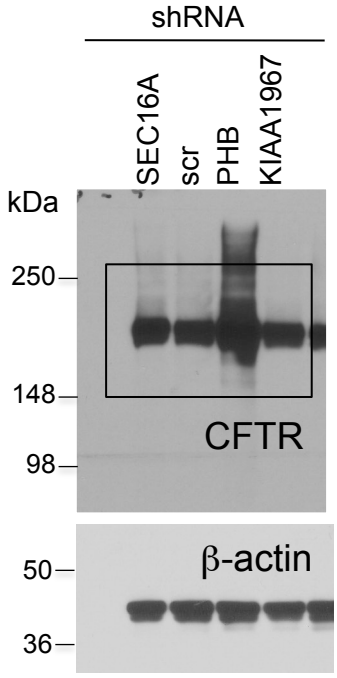

Extended Data Fig. 5

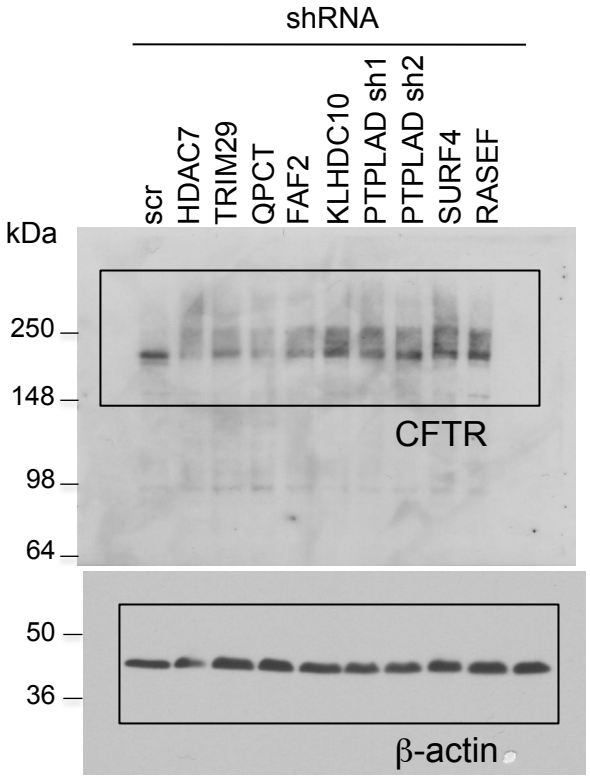

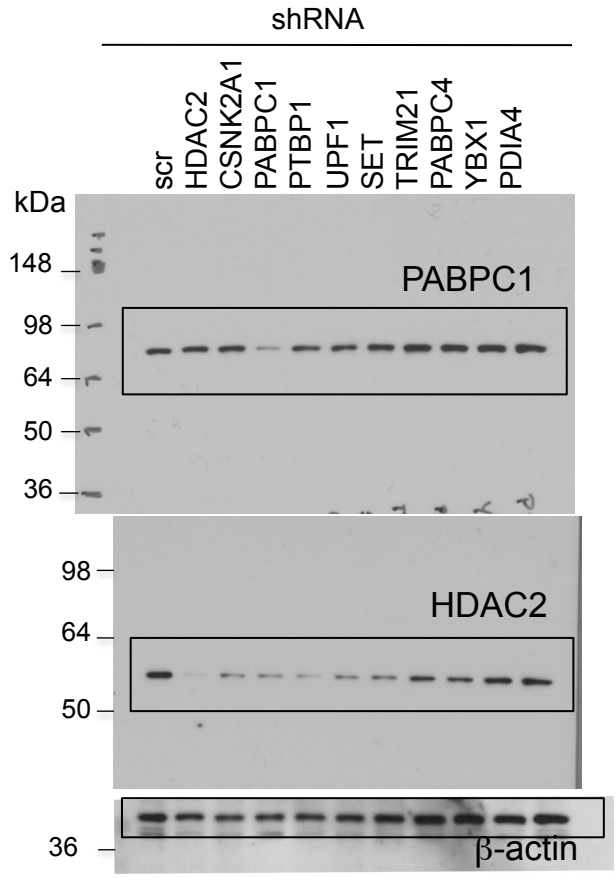

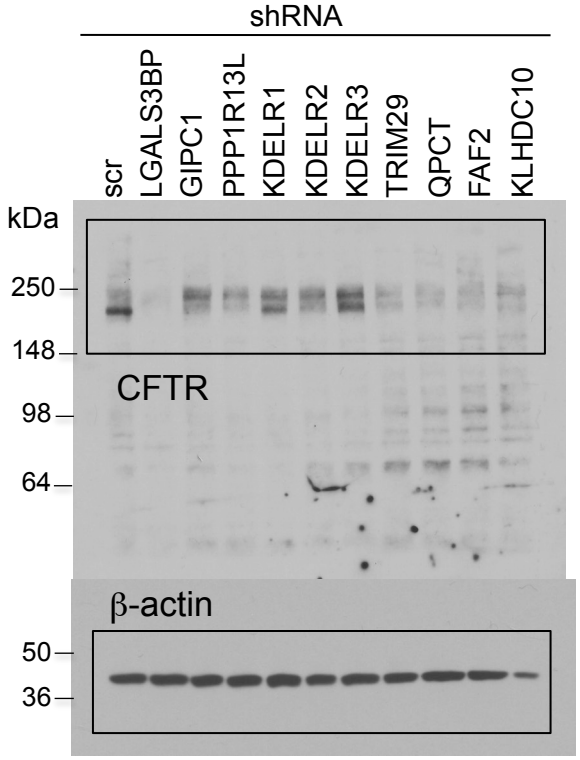

Extended Data Fig. 7c

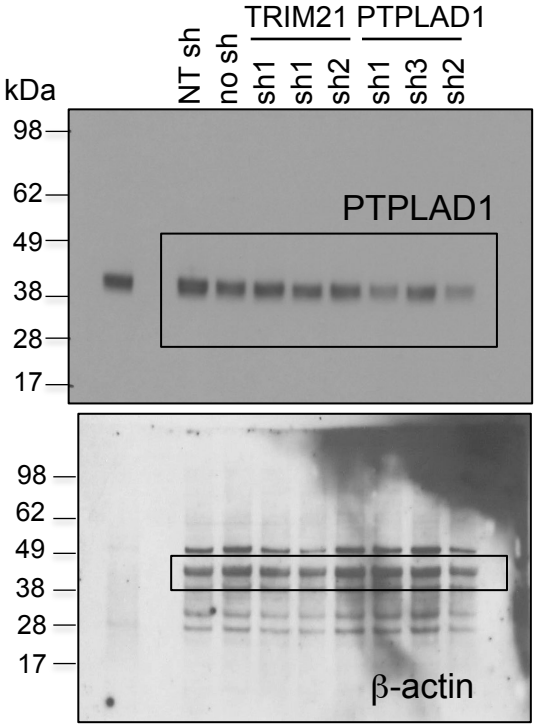

Extended Data Fig. 7c

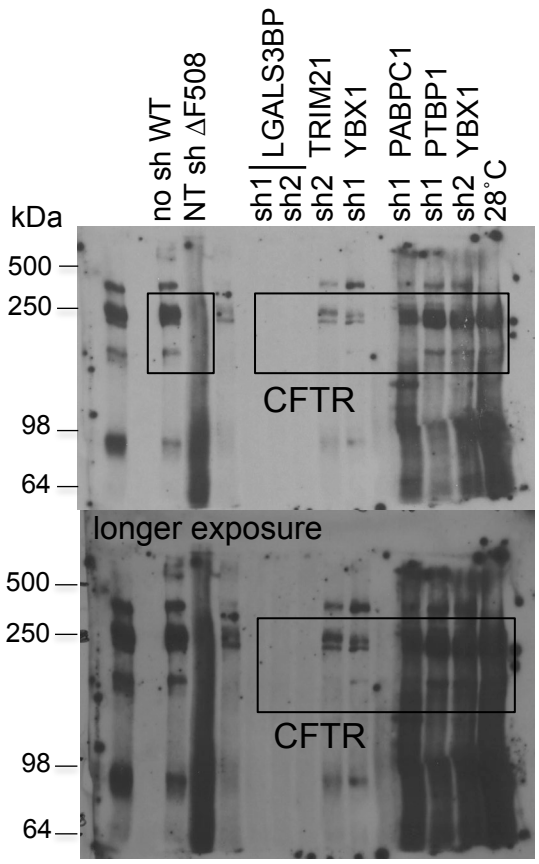

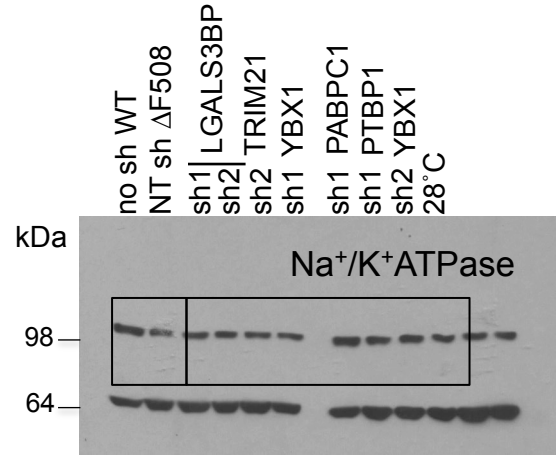

Same samples reloaded as above on a different blot

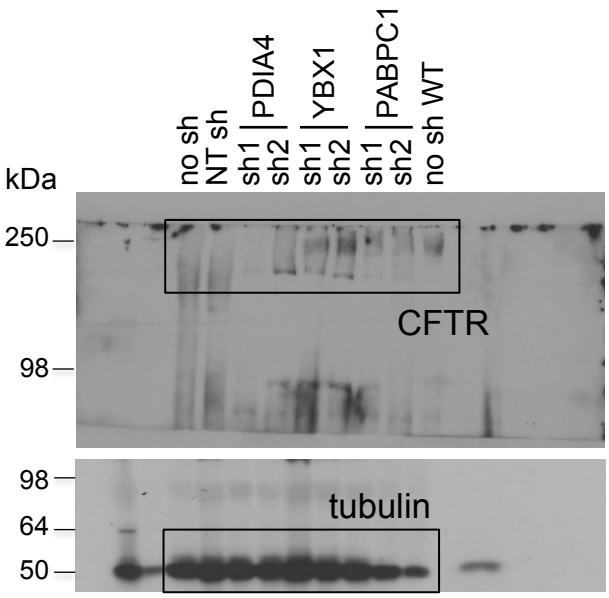

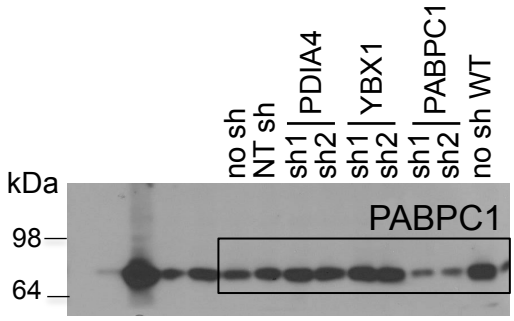

Same samples reloaded as above on a different blot

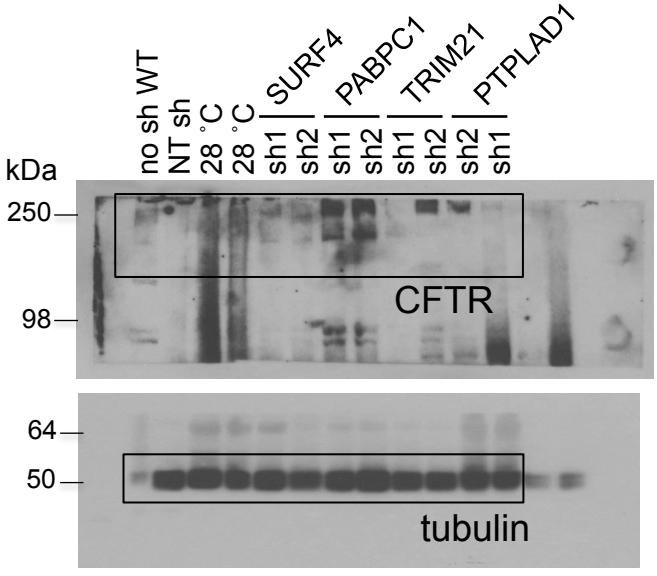

Extended Data Fig. 7c

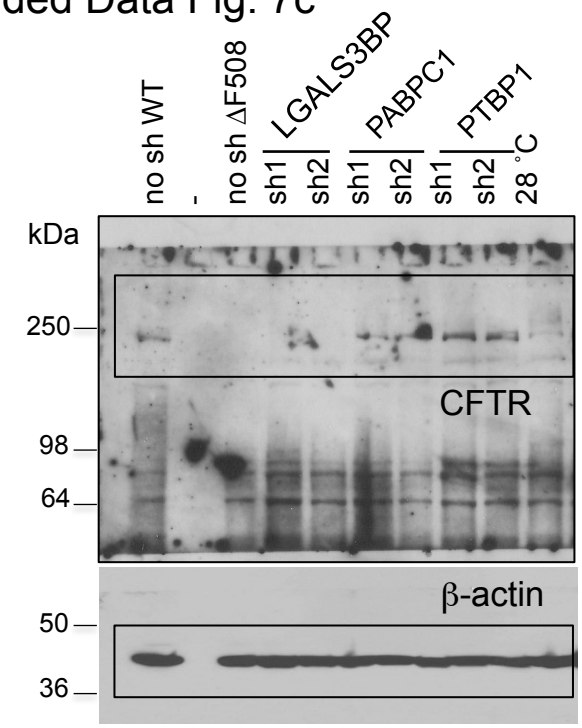

Extended Data Fig. 8b

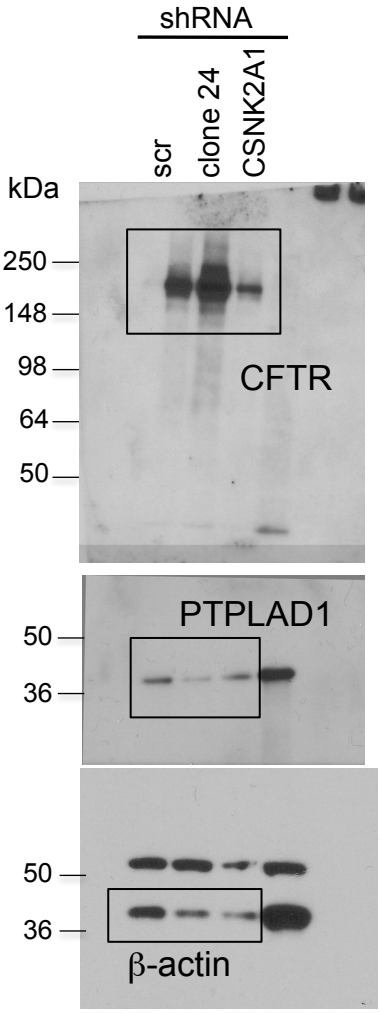

Extended Data Fig. 8b